DOI 10.2478/ama-2021-0012

APPROXIMATE FORMULATION OF THE RIGID BODY MOTIONS OF AN ELASTIC RECTANGLE UNDER SLIDING BOUNDARY CONDITIONS

Onur ŞAHİN[*], Barış ERBAŞ[**], Brent WILSON[***],

[*]Department of Mathematics, Giresun University, Gaziler, Prof. Ahmet Taner Kışlalı Cd., 28200 Giresun Turkey
[**]Department of Mathematics, Eskişehir Technical University, 2 Eylül Kampüsü, 26555 Eskişehir, Turkey
[***] HUM Industrial Technology, INC, 911 Washington Ave, Suite 501 St. Louis, Missouri, USA

onur.sahin@giresun.edu.tr, berbas@eskisehir.edu.tr, bwilson@humindustrial.com

received 15 February 2021, revised 31 May 2021, accepted 7 June 2021

Abstract: Low-frequency analysis of in-plane motion of an elastic rectangle subject to end loadings together with sliding boundary conditions is considered. A perturbation scheme is employed to analyze the dynamic response of the elastic rectangle revealing nonhomogeneous boundary-value problems for harmonic and biharmonic equations corresponding to leading and next order expansions, respectively. The solution of the biharmonic equation obtained by the separation of variables, a consequence of sliding boundary conditions, gives an asymptotic correction to the rigid body motion of the rectangle. The derived explicit approximate formulae are tested for different kinds of end loadings together with numerical examples demonstrating the comparison against the exact solutions.

Key words: elastic rectangle, low-frequency, rigid body motion, perturbation scheme, sliding boundary conditions

1. INTRODUCTION

Dynamics of elastic structures, an important branch of solid mechanics, is of interest in several studies encountered in modern industrial applications (see Qin et al., 2008; Martin et al., 2012; Wang, 2014; Kudaibergenov et al., 2016; Viverge et al., 2016). Because most efforts in determining the exact formulations for displacement components and frequencies of such structures generally result in intricate transcendental relations, developing mathematical models that reveal the eigenfrequencies of the system from the traditional equations of rigid body dynamics has become an important endeavor in this area. A considerable number of studies in recent years, therefore, have focused on developing perturbation approaches allowing further insight into the dynamic response of considered elastic structures, e.g., (Kaplunov et al., 2019) and (Kaplunov and Şahin, 2020). It is well known that the conventional equations of rigid body motion are also an application of Newtonian mechanics to elastic solids. We mention (Milton and Willis, 2007) that suggest a new methodology leading to a better approximation of Newton's second law of motion for macroscopic rigid bodies. A distinguished elastodynamic homogenization theory for periodic and random inhomogeneous media was presented in (Srivastava and Nemat-Nasser, 2012; Willis, 1981a; Willis, 1981b), including effective constitutive relations that are nonlocal in space and time.

The self-equilibrated loading, the effect of which is generally omitted by classical rigid body dynamics may be important for various applications, e.g., longitudinal railway dynamics (see Kaplunov et al., 2015). Here, the self-equilibrium is not meant in the sense of Saint-Venant's principle for elastic structures, e.g., (Vigak and Tokovyi, 2002), see also (Gregory and Wan, 1985), and (Kaplunov et al., 2021) adapting this principle for deriving boundary conditions in thin plate theory, but for the setup in which the end forces applied have the resultants of the same amplitude but different direction. A low-frequency analysis of a viscoelastic inhomogeneous bar under the action of end loads, also inspired by modeling of railcar dynamics, is considered in (Kaplunov et al., 2015), and explicit asymptotic corrections to the conventional equations of rigid body motion are presented. We also mention almost rigid body motions of a system consisting of strongly inhomogeneous elastic beams considered in (Şahin, 2019) and (Şahin et al., 2020).

In this paper, we construct a correction to Newton's second law for an elastic rectangle subject to sliding boundary conditions in case of low-frequency motion related to a typical time scale that is assumed to be much greater than the time elastic waves that take the distance between the opposite sides of the rectangle. A perturbation scheme developed in terms of a small parameter associated with low-frequency is used to obtain a generalized formulation for displacements of the elastic rectangle under the influence of edge loadings. The asymptotic study of similar boundary-value problems, such as response of a semi-infinite rectangle to end loadings, usually agree with the Saint-Venant's principle that states that statically self-equilibrated loads cause only local disturbances that do not propagate far away from a loaded area (see Babenkova and Kaplunov, 2004 and Babenkova et al., 2005).

The paper is organized as follows. In Section 2, the statement of in-plane dynamic problem for an elastic rectangle subject to sliding boundary conditions is presented. The governing equations and scaling of the parameters are given. Section 3 contains a perturbation procedure that formulates the problem with the help of a small parameter arising from the definition of the low-frequency of the rectangle. In Section 4, illustrative examples for

the developed model are given, and numerical computations comparing the exact and approximate formulations are presented. Conclusions are given in the last section.

2. STATEMENT OF THE PROBLEM

The in-plane dynamic problem for a linear, isotropic elastic rectangle under the action of edge loads and subject to sliding boundary conditions is considered in the framework of linear elasticity, see Fig. 1.

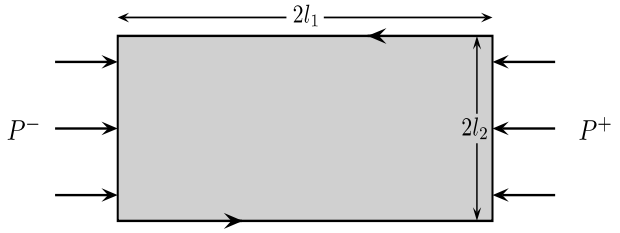

Fig. 1. An elastic rectangle under the considered edge loading and sliding support

In-plane motions of the isotropic rectangle are governed by the equations of two-dimensional elasticity:

$$\sigma_{ij,j} = \rho u_{i,tt} \ , \quad i,j = 1,2 \tag{1}$$

where u_i are in-plane displacement components, σ_{ij} are stress tensor components, t is time, and ρ is mass density. The edge loadings and the sliding boundary conditions on the faces of rectangle are written, respectively, as:

$$\begin{aligned} &\sigma_{11}(\pm l_1, x_2, t) = P^{\pm}, \quad \sigma_{12}(\pm l_1, x_2, t) = 0, \\ &\sigma_{21}(x_1, \pm l_2, t) = 0, \quad u_2(x_1, \pm l_2, t) = 0. \end{aligned} \tag{2}$$

It is natural to separate the solution in symmetric and antisymmetric parts. For simplicity, we consider only the symmetric part whereas the antisymmetric part may be investigated similarly. Therefore, it is assumed that $P^{\pm} = P^{\pm}(x_2, t)$ are even in x_2. The constitutive equations relating the stress and displacement components are expressed through:

$$\begin{aligned} &\sigma_{ii} = \frac{E(1-\nu)}{(1+\nu)(1-2\nu)}\, u_{i,i} + \frac{E\nu}{(1+\nu)(1-2\nu)} u_{j,j}, \\ &\sigma_{ij} = \frac{E}{2(1+\nu)}(u_{i,j} + u_{j,i}), \quad i \neq j = 1,2. \end{aligned} \tag{3}$$

where E is Young's modulus and ν is Poisson's ratio.

Our main concern is the low-frequency motions of the rectangle under plane strain conditions that suggest introducing the small parameter η defined by:

$$\eta = \frac{l_1}{T c_2} \ll 1, \tag{4}$$

and rescaling the problem in the nondimensional quantities introduced in the form:

$$\begin{aligned} &\sigma_{ij}^* = \frac{\sigma_{ij}}{\eta^2 \rho\, c_2^2}, \quad u_i^* = \frac{u_i}{l_1}, \quad P_*^{\pm} = \frac{P^{\pm}}{\eta^2 \rho\, c_2^2}, \\ &y_i = \frac{x_i}{l_i}, \quad \tau = \frac{t}{T}, \quad i,j = 1,2. \end{aligned} \tag{5}$$

Here, $c_2 = \sqrt{E/2\rho(1+\nu)}$ denotes the transverse wave speed and T is a typical time scale grater than the longitudinal and transverse waves to propagate the distance equal to the thickness of the body.

Formulae (1) and (3) may, therefore, be rewritten as:

$$\begin{aligned} &\sigma_{11,1}^* + \delta \sigma_{12,2}^* = u_{1,\tau\tau}^*, \\ &\sigma_{12,1}^* + \delta \sigma_{22,2}^* = u_{2,\tau\tau}^*, \end{aligned} \tag{6}$$

and:

$$\begin{aligned} &\eta^2 \sigma_{11}^* = \kappa^2\, u_{1,1}^* + \delta\, (\kappa^2 - 2) u_{2,2}^*, \\ &\eta^2 \sigma_{12}^* = \delta\, u_{1,2}^* + u_{2,1}^*, \\ &\eta^2 \sigma_{22}^* = \delta\, \kappa^2\, u_{2,2}^* + (\kappa^2 - 2)\, u_{1,1}^* \end{aligned} \tag{7}$$

where $\delta = l_1/l_2$ and $\kappa^2 = 2(1-\nu)/(1-2\nu)$.

3. PERTURBATION PROCEDURE

We seek the solution $\{u_i, \sigma_{ij}\}$ of the boundary-value problems (6) to (7) in the form of the following asymptotic series:

$$\begin{aligned} &u_i^* = u_i^{(0)} + \eta^2 u_i^{(1)} + \cdots, \\ &\sigma_{ii}^* = \sigma_{ii}^{(0)} + \eta^2 \sigma_{ii}^{(1)} + \cdots, \\ &\sigma_{ij}^* = \sigma_{ij}^{(0)} + \eta^2 \sigma_{ij}^{(1)} + \cdots, \quad i \neq j = 1,2. \end{aligned} \tag{8}$$

On substituting expansions (8) into the governing equations (6) and the constitutive relations (7), the leading order displacements, that is the first components in expansions (8) independent of the powers of η are governed by the boundary-value problem given by:

$$\begin{aligned} &\sigma_{11,1}^{(0)} + \delta \sigma_{12,2}^{(0)} = u_{1,\tau\tau}^{(0)}, \\ &\sigma_{12,1}^{(0)} + \delta \sigma_{22,2}^{(0)} = u_{2,\tau\tau}^{(0)}, \end{aligned} \tag{9}$$

with:

$$\begin{aligned} &\kappa^2\, u_{1,1}^{(0)} + \delta\, (\kappa^2 - 2)\, u_{2,2}^{(0)} = 0, \\ &\delta\, u_{1,2}^{(0)} + u_{2,1}^{(0)} = 0, \\ &\delta\, \kappa^2\, u_{2,2}^{(0)} + (\kappa^2 - 2)\, u_{1,1}^{(0)} = 0, \end{aligned} \tag{10}$$

and:

$$\begin{aligned} &\sigma_{11}^{(0)}\big|_{y_1 = \pm 1} = P_*^{\pm}, \qquad \sigma_{12}^{(0)}\big|_{y_1 = \pm 1} = 0 \\ &\sigma_{21}^{(0)}\big|_{y_2 = \pm 1} = 0, \qquad u_2^{(0)}\big|_{y_2 = \pm 1} = 0. \end{aligned} \tag{11}$$

Eqns. (10_1) and (10_3) yield that:

$$u_{i,i}^{(0)} = 0, \quad i = 1,2 \tag{12}$$

resulting in:

$$u_1^{(0)} = u_1^{(0)}(y_2, \tau), \quad u_2^{(0)} = u_2^{(0)}(y_1, \tau). \tag{13}$$

Substituting (13) into the second equation of (10) gives the final form of the leading order displacements, that is:

$$u_i^{(0)} = U_i(\tau), \quad i = 1,2. \tag{14}$$

Due to boundary condition (10_3), the second component of

leading order displacement vanishes, i.e.,

$$u_2^{(0)} = 0. \tag{15}$$

Thus, equations (9_1) and (9_2) become:

$$\begin{aligned} &\sigma_{11,1}^{(0)} + \delta\sigma_{12,2}^{(0)} = U_{1,\tau\tau}, \\ &\sigma_{12,1}^{(0)} + \delta\sigma_{22,2}^{(0)} = 0. \end{aligned} \tag{16}$$

Integrating (16_1) over the rectangular region we derive, employing boundary conditions (11):

$$\begin{aligned} &\int_{-1}^{1}\int_{-1}^{1} \frac{\partial\sigma_{11}^{(0)}}{\partial y_1} dy_1 dy_2 + \delta \int_{-1}^{1}\int_{-1}^{1} \frac{\partial\sigma_{12}^{(0)}}{\partial y_2} dy_2 dy_1 = \\ &= \int_{-1}^{1} \left(\sigma_{11}^{(0)}\big|_{y_1=1} - \sigma_{11}^{(0)}\big|_{y_1=-1}\right) dy_2 \\ &+\delta \int_{-1}^{1} \left(\sigma_{12}^{(0)}\big|_{y_2=1} - \sigma_{12}^{(0)}\big|_{y_2=-1}\right) dy_1 \\ &= \int_{-1}^{1} (P_*^+ - P_*^-) dy_2 = 4U_{1,\tau\tau}. \end{aligned} \tag{17}$$

We, therefore, have at leading order:

$$u_{1,\tau\tau}^{(0)} = \frac{1}{4}\int_{-1}^{1} (P_*^+ - P_*^-) dy_2 \tag{18}$$

which is in agreement with Newton's second law:

$$m\, u_{1,\tau\tau} = \frac{1}{4}\int_{-l_2}^{l_2} (\mathrm{P}^+ - \mathrm{P}^-) dx_2 \tag{19}$$

where $m = l_1 l_2 \rho$, see (Kaplunov and Şahin, 2020).

Next order boundary-value problem may be expressed through the pseudo-static equations given by:

$$\begin{aligned} &\kappa^2 \frac{\partial^2 u_1^{(1)}}{\partial y_1^2} + \delta^2 \frac{\partial^2 u_1^{(1)}}{\partial y_2^2} + \delta(\kappa^2 - 1)\frac{\partial^2 u_2^{(1)}}{\partial y_1 \partial y_2} = u_{1,\tau\tau,}^{(0)} \\ &\delta^2\kappa^2 \frac{\partial^2 u_2^{(1)}}{\partial y_2^2} + \frac{\partial^2 u_2^{(1)}}{\partial y_1^2} + \delta(\kappa^2 - 1)\frac{\partial^2 u_1^{(1)}}{\partial y_1 \partial y_2} = 0 \end{aligned} \tag{20}$$

with:

$$\begin{aligned} &\kappa^2\, u_{1,1}^{(1)} + \delta\,(\kappa^2 - 2) u_{2,2}^{(1)}\big|_{y_1=\pm 1} = P_*^{\pm}, \\ &\delta\, u_{1,2}^{(1)} + u_{2,1}^{(1)}\big|_{y_1=\pm 1} = 0, \\ &\delta\, u_{1,2}^{(1)} + u_{2,1}^{(1)}\big|_{y_2=\pm 1} = 0, \\ &u_2^{(1)}\big|_{y_2=\pm 1} = 0. \end{aligned} \tag{21}$$

Let us consider solutions of eqn. (20) in the form:

$$u_1^{(1)} = X_{10}(y_1) + \sum_{n=1}^{\infty} X_{1n}(y_1)\cos n\pi y_2, \tag{22}$$

$$u_2^{(1)} = \sum_{n=1}^{\infty} X_{2n}(y_1)\sin n\pi y_2.$$

Substituting the assumed form of the next order displacements (22) into the governing equations (20) yield:

$$\begin{aligned} &\kappa^2\left(X_{10}'' + \sum_{n=1}^{\infty} X_{1n}''\cos n\pi y_2\right) - \\ &-\delta^2 \sum_{n=1}^{\infty} (n\pi)^2 X_{1n}\cos n\pi y_2 + \\ &+\delta(\kappa^2 - 1)\sum_{n=1}^{\infty} (n\pi) X_{2n}'\cos n\pi y_2 = \\ &= \frac{a_0}{2} + \sum_{n=1}^{\infty} a_n\cos n\pi y_2 + b_n\cos n\pi y_2, \end{aligned} \tag{23}$$

and:

$$\begin{aligned} &-\delta^2\kappa^2 \sum_{n=1}^{\infty} (n\pi)^2 X_{2n} \sin n\pi y_2 + \\ &+\sum_{n=1}^{\infty} X_{2n}'' \sin n\pi y_2 - \\ &-\delta(\kappa^2 - 1)\sum_{n=1}^{\infty} (n\pi) X_{1n}' \sin n\pi y_2 = 0 \end{aligned} \tag{24}$$

where:

$$\begin{aligned} &\mathrm{a}_0 = \int_{-1}^{1} p\, dy_2 = 2p, \\ &\mathrm{a}_n = \int_{-1}^{1} p\cos n\pi y_2\, dy_2, \\ &b_n = \int_{-1}^{1} p\sin n\pi y_2\, dy_2, \end{aligned} \tag{25}$$

with:

$$p = \frac{1}{4}\int_{-1}^{1} (P_*^+ - P_*^-) dy_2 \tag{26}$$

which is a constant function. Equations (23) and (24) may be reduced, on using (25) and (26), to the differential equations:

$$\kappa^2 X_{10}'' = \frac{a_0}{2} = p \tag{27}$$

and:

$$\begin{aligned} &\kappa^2 X_{1n}'' - \delta^2 (n\pi)^2 X_{1n} + \delta(\kappa^2 - 1)(n\pi) X_{2n}' = 0, \\ &-\delta^2\kappa^2 (n\pi)^2 X_{2n} + X_{2n}'' - \delta(\kappa^2 - 1)(n\pi) X_{1n}' = 0, \end{aligned} \tag{28}$$

where the term-wise equality of Fourier series is utilized.

The solution of eqn. (27) may clearly be written as:

$$X_{10} = \frac{p}{\kappa^2} A_{10} y_1^2 + A_{20} y_1 + A_{30}. \tag{29}$$

It can also be seen from (28_1) that:

$$X_{2n}{}' = -\frac{\kappa^2}{\delta(\kappa^2-1)(n\pi)} X_{1n}{}'' + \frac{\delta^2 (n\pi)^2}{\delta(\kappa^2-1)(n\pi)} X_{1n}. \tag{30}$$

Taking the derivative of (28_2) with respect to y_1 and using (30) we obtain:

$$X_{1n}^{(\mathrm{iv})} - 2(\delta n\pi)^2 X_{1n}{}'' + (\delta n\pi)^4 X_{1n} = 0 \tag{31}$$

The solution of which may be written as:

$$X_{1n} = (A_1 + \delta n\pi y_1 A_2)\sinh\delta n\pi y_1 + \\ +(A_3 + \delta n\pi y_1 A_4)\cosh\delta n\pi y_1. \tag{32}$$

Substituting (32) into the differential relation (30) results in:

$$X_{2n}' = -\delta n\pi \sinh(\delta n\pi y_1) A_1 - \delta n\pi \cosh(\delta n\pi y_1) A_3 - \\ - \frac{\delta n\pi (2\kappa^2 \cosh(\delta n\pi y_1) + \delta n\pi y_1 (\kappa^2-1)\sinh(\delta n\pi y_1))}{\kappa^2-1} \\ - \frac{\delta n\pi (2\kappa^2 \sinh(\delta n\pi y_1) + \delta n\pi y_1 (\kappa^2-1)\cosh(\delta n\pi y_1))}{\kappa^2-1}$$

which yields:

$$X_{2n} = -\cosh(\delta n\pi y_1) A_1 - \sinh(\delta n\pi y_1) A_3 - \\ - \left(\delta n\pi y_1 \cosh(\delta n\pi y_1) + \frac{(\kappa^2+1)\sinh(\delta n\pi y_1)}{\kappa^2-1} \right) A_2 - \\ - \left(\delta n\pi y_1 \sinh(\delta n\pi y_1) + \frac{(\kappa^2+1)\cosh(\delta n\pi y_1)}{\kappa^2-1} \right) A_4. \tag{33}$$

The displacements may consequently be written as:

$$u_1^{(1)} = \frac{p}{\kappa^2} A_{10} y_1^2 + A_{20} y_1 + A_{30} + \\ + \sum_{n=1}^{\infty} \{(A_1 + \delta n\pi y_1 A_2)\sinh\delta n\pi y_1 + \\ +(A_3 + \delta n\pi y_1 A_4)\cosh\delta n\pi y_1\} \cos n\pi y_2 \tag{34}$$

and:

$$u_2^{(1)} = \sum_{n=1}^{\infty} -\cosh(\delta n\pi y_1) A_1 - \sinh(\delta n\pi y_1) A_3 - \\ - \left(\delta n\pi y_1 \cosh(\delta n\pi y_1) + \frac{(\kappa^2+1)\sinh(\delta n\pi y_1)}{\kappa^2-1} \right) A_2 - \\ - \left(\delta n\pi y_1 \sinh(\delta n\pi y_1) + \frac{(\kappa^2+1)\cosh(\delta n\pi y_1)}{\kappa^2-1} \right) A_4 \} \sin n\pi y_2. \tag{35}$$

Boundary condition (21) may be written as:

$$\kappa^2 u_{1,1}^{(1)} + \delta(\kappa^2-2) u_{2,2}^{(1)}\big|_{y_1=\pm 1} = \frac{B_0^{\pm}}{2} + \\ + \sum_{n=1}^{\infty} B_n^{\pm} \cos n\pi y_2 + C_n^{\pm} \sin n\pi y_2, \\ \delta u_{1,2}^{(1)} + u_{2,1}^{(1)}\big|_{y_1=\pm 1} = 0, \\ \delta u_{1,2}^{(1)} + u_{2,1}^{(1)}\big|_{y_2=\pm 1} = 0, \\ u_2^{(1)}\big|_{y_2=\pm 1} = 0 \tag{36}$$

where:

$$B_0^{\pm} = \int_{-1}^{1} P_*^{\pm} dy_2, \\ B_n^{\pm} = \int_{-1}^{1} P_*^{\pm} \cos n\pi y_2 \, dy_2, \\ C_n^{\pm} = \int_{-1}^{1} P_*^{\pm} \sin n\pi y_2 \, dy_2. \tag{37}$$

On employing, the displacements (34) and (35) in the boundary conditions (36) yield, respectively, the following equations for X_{10}, X_1 and X_2:

$$\kappa^2 \frac{\partial X_{10}}{\partial y_1}\Big|_{y_1=\pm 1} = \frac{1}{2} \int_{-1}^{1} P_*^{\pm} dy_2 \tag{38}$$

and:

$$\kappa^2 \sum_{n=1}^{\infty} X_{1n}'(y_1) \cos n\pi y_2 + \\ + \delta(\kappa^2-2) n\pi \sum_{n=1}^{\infty} X_{2n}(y_1) \cos n\pi y_2 |_{y_1=\pm 1} = \\ = \sum_{n=1}^{\infty} B_n^{\pm} \cos n\pi y_2 + C_n^{\pm} \sin n\pi y_2, \\ - \delta\kappa^2 n\pi \sum_{n=1}^{\infty} X_{1n}(y_1) \sin n\pi y_2 + \\ + \sum_{n=1}^{\infty} X_{2n}'(y_1) \sin n\pi y_2 |_{y_1=\pm 1} = 0 \tag{39}$$

resulting in:

$$\kappa^2 X_{1n}'(y_1) + \delta(\kappa^2-2) n\pi X_{2n}(y_1)|_{y_1=\pm 1} \\ = \int_{-1}^{1} P_*^{\pm} \cos n\pi y_2 \, dy_2, \\ -\delta\kappa^2 n\pi X_{1n}(y_1) + X_{2n}{}'(y_1)|_{y_1=\pm 1} = 0. \tag{40}$$

All coefficients appearing in the displacements $u_1^{(1)}$ and $u_2^{(1)}$, see (34) and (56), may be calculated substituting expressions (29), (32) and (33) into equation (40), which gives:

$$A_{10} = \frac{1}{2}, \tag{41}$$

$$A_{20} = \frac{1}{4\kappa^2}\int_{-1}^{1}(P_*^+ + P_*^-)dy_2,$$

and:

$$A_1 = \frac{\cosh(\delta n\pi)(\delta n\pi(\kappa^2-1)+\kappa^2\tanh(\delta n\pi))}{2\delta n\pi(\kappa^2-1)(2\delta n\pi+\sinh(2\delta n\pi))}I_1,$$
$$A_2 = \frac{\cosh(\delta n\pi)}{2\delta n\pi(2\delta n\pi-\sinh(2\delta n\pi))}\ I_2,$$
$$A_3 = -\frac{\cosh(\delta n\pi)\ (\kappa^2+\delta n\pi(\kappa^2-1)\tanh(\delta n\pi))}{2\delta n\pi(\kappa^2-1)(2\delta n\pi-\sinh(2\delta n\pi))}\ I_2, \quad (42)$$
$$A_4 = -\frac{\sinh(\delta n\pi)}{2\delta n\pi(2\delta n\pi+\sinh(2\delta n\pi))}\ I_1,$$

where:

$$\mathrm{I}_1 = \int_{-1}^{1}(P_*^+ + P_*^-)\cos n\pi y_2\, dy_2,$$
$$\mathrm{I}_2 = \int_{-1}^{1}(P_*^+ - P_*^-)\cos n\pi y_2\, dy_2. \quad (43)$$

A higher order approximation is still needed to determine the coefficient A_{30}. To this end, starting from (6) and (34), we write:

$$\sigma_{11,1}^{(1)} + \delta\sigma_{12,2}^{(1)} = u_{1,\tau\tau}^{(1)} \quad (44)$$

with:

$$\sigma_{11}^{(1)}\big|_{y_1=\pm1} = \sigma_{12}^{(1)}\big|_{y_2=\pm1} = 0. \quad (45)$$

Integrating equation (44) over the rectangular region and using boundary condition (45), we obtain:

$$A_{30} = -\frac{p}{6\kappa^2}. \quad (46)$$

Thus, the expressions for the next order displacements $u_1^{(1)}$ and $u_2^{(1)}$ are fully established. The following section aims to present demonstrative examples.

4. ILLUSTRATIVE EXAMPLES

4.1. Time-Harmonic Loadings of Parabolic Types

First, we consider time-harmonic, parabolic type end loadings given by:

$$P^{\pm} = M^{\pm}(1 - x_2^2/l_2^2)e^{-i\omega t} \quad (47)$$

where $M^{\pm}$ is a constant amplitude. Below, we utilize the scaling introduced in (5) and also omit the time-harmonic factor $e^{-i\omega t}$. It is, therefore, an easy matter to obtain the tangential displacement using (18), which is:

$$u_1^{(0)} = -\frac{M_*^+ - M_*^-}{3} \quad (48)$$

where $M_*^{\pm}$ is scaled as in (5).

The solution of the next order problem may be written from eqns. (34) and (35) as:

$$u_1^{(1)} = \frac{M_*^+ - M_*^-}{6\kappa^2}y_1^2 + \frac{M_*^+ + M_*^-}{3\kappa^2}y_1 - \frac{M_*^+ - M_*^-}{18\kappa^2} + \\ + \sum_{n=1}^{\infty}\{(D_1 + \delta n\pi y_1 D_2)\sinh\delta n\pi y_1 + \\ +(D_3 + \delta n\pi y_1 D_4)\cosh\delta n\pi y_1\}\cos n\pi y_2 \quad (49)$$

and:

$$u_2^{(1)} = \sum_{n=1}^{\infty}\{-\cosh(\delta n\pi y_1)D_1 - \sinh(\delta n\pi y_1)D_3 - \\ -\left(\delta n\pi y_1\cosh(\delta n\pi y_1) + \frac{(\kappa^2+1)\sinh(\delta n\pi y_1)}{\kappa^2-1}\right)D_2 - \\ -\left(\delta n\pi y_1\sinh(\delta n\pi y_1) + \frac{(\kappa^2+1)\cosh(\delta n\pi y_1)}{\kappa^2-1}\right)D_4\Big\}\sin n\pi y_2 \quad (50)$$

where:

$$D_1 = \frac{(-1)^{n+1}2(M_*^+ + M_*^-)\cosh(\delta n\pi)}{\delta n^3\pi^3(\kappa^2-1)(2\delta n\pi+\sinh(2\delta n\pi))}\times \\ \times(\delta n\pi(\kappa^2-1)+\kappa^2\tanh(\delta n\pi)),$$
$$D_2 = \frac{(-1)^{n+1}2(M_*^+ - M_*^-)\cosh(\delta n\pi)),}{\delta n^3\pi^3(2\delta n\pi-\sinh(2\delta n\pi))}$$
$$D_3 = \frac{(-1)^{n}2(M_*^+ - M_*^-)\cosh(\delta n\pi))}{\delta n^3\pi^3(\kappa^2-1)(2\delta n\pi-\sinh(2\delta n\pi))}\times \\ \times(\kappa^2+\delta n\pi(\kappa^2-1)\tanh(\delta n\pi)), \quad (51)$$
$$D_4 = \frac{(-1)^{n}2(M_*^+ + M_*^-)\sinh(\delta n\pi)}{\delta n^3\pi^3(2\delta n\pi+\sinh(2\delta n\pi))}.$$

In the following figures, we illustrate the comparisons of approximate and exact longitudinal displacement u_1 given, respectively, by formulas (49) and (60). Here, we set the Poisson ratio $\nu = 0.25$ together with $\delta = 1$. Figures 2 and 3 illustrate the behavior of the approximate and exact displacement component u_1 along the longitudinal coordinate y_1 under the action of self-equilibrated and non-self-equilibrated loads, that is, we take $M_*^+ = M_*^- = 1$ and $M_*^+ = -M_*^- = 1$, respectively. An excellent agreement is evident for the parameter η, even when its value is not very small.

In both of these figures, we consider only positive y_2-values due to the intrinsic symmetry. The largest displacements occur along the y_1-axis, while they decrease in the y_2-direction due to the form of the applied loads. However, for a self-equilibrated load, Fig. 2, there is no displacement along the y_2-axis, i.e., at $y_1 = 0$, which is not observed in the case of a non-self-equilibrated load, see Fig 3.

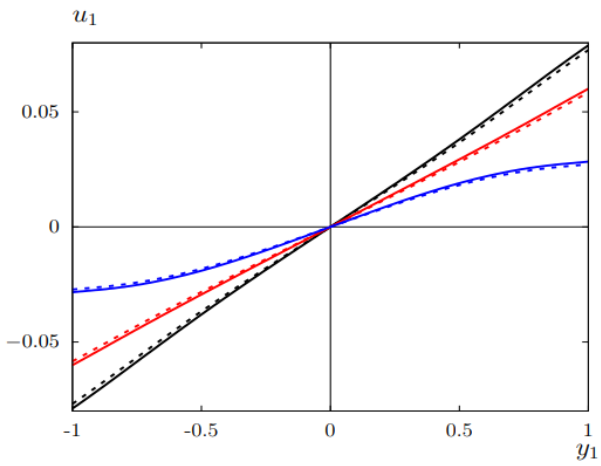

Fig. 2. Comparison of exact (solid lines) and approximate (dotted lines) displacements u_1 versus y_1 for $y_2 = 0$ (black), $y_2 = 0.5$ (red), and $y_2 = 1$ (blue) in case of a self-equilibrated load at $\eta = 0.5$

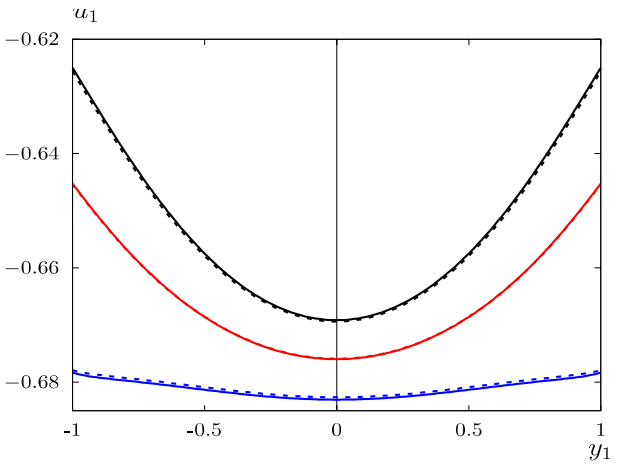

Fig. 3. Comparison of exact (solid lines) and approximate (dotted lines) displacements u_1 versus y_1 for $y_2 = 0$ (black), $y_2 = 0.5$ (red), and $y_2 = 1$ (blue) in case of a non-self-equilibrated load at $\eta = 0.5$

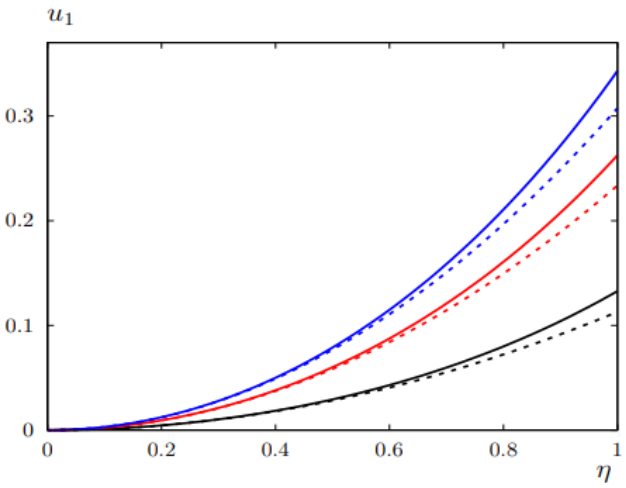

Fig. 4. Comparison of exact (solid lines) and approximate (dotted lines) displacements u_1 versus η for $y_1 = y_2 = 0.5$ (black), $y_1 = 1$, $y_2 = 0.5$ (red), and $y_1 = 1$, $y_2 = 0$ (blue) in case of a self-equilibrated load

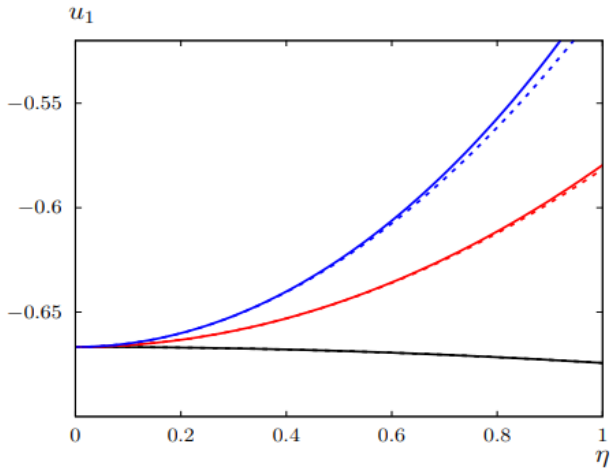

Fig. 5. Comparison of exact (solid lines) and approximate (dotted lines) displacements u_1 versus η for $y_1 = y_2 = 0.5$ (black), $y_1 = 1$, $y_2 = 0.5$ (red), and $y_1 = 1$, $y_2 = 0$ (blue) in case of a non-self-equilibrated load

Figures 4 and 5 demonstrate the variations of the longitudinal displacement with respect to the small frequency η in case of self- and non-self-equilibrated loads, respectively. A remarkable coincidence between the approximate and exact displacements is observed even in the global low-frequency regime. When the load is self-equilibrated, we observe from Fig. 4 that at very low frequencies the horizontal displacement u_1 acquires considerably small values both along the y_1-axis ($y_2 = 0$) as well as in the vertical direction. As the frequency increases, the horizontal displacement attains larger values that also increase in the positive vertical direction. For a non-self-equilibrated load, the displacements for the considered points are not small even for low-frequency regime. The displacement characteristics are also quite different than the previous case, clearly a result of non-self-equilibrated loading.

4.1. Time-Harmonic Uniform Loading

We now consider time-harmonic, uniform end loadings in the form:

$$P^{\pm} = A^{\pm} e^{-i\omega t} \tag{52}$$

where $A^{\pm}$ are again assumed to be constants. On using eqn. (18) and omitting $e^{-i\omega t}$, the leading order displacement may be obtained as:

$$u_1^{(0)} = -\frac{A_*^+ - A_*^-}{2}. \tag{53}$$

Similar to previous section, the next order solution for the displacement components may be written as

On substituting expansions (8) into the governing equations (6) and the constitutive relations (7), the leading order displacements, that:

$$u_1^{(1)} = \frac{A_*^+ - A_*^-}{4\kappa^2} y_1^2 + \frac{A_*^+ + A_*^-}{2\kappa^2} y_1 - \frac{A_*^+ - A_*^-}{12\kappa^2}, \tag{54}$$

and:

$$u_2^{(1)} = 0 \tag{55}$$

since each coefficient given in (43) becomes zero.

DOI 10.2478/ama-2021-0012

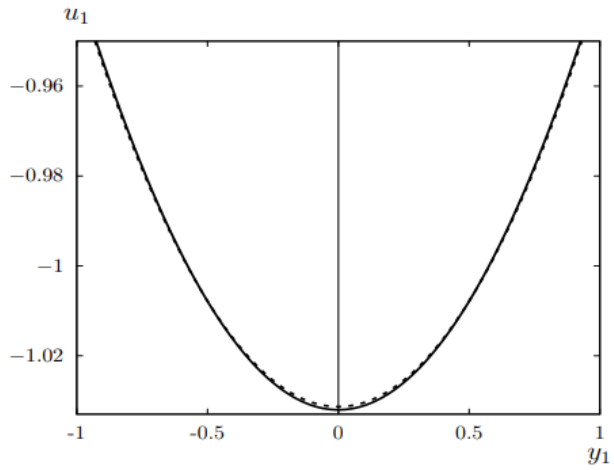

Fig. 6. Comparison of exact (solid lines) and approximate (dotted lines) displacements u_1 versus y_1 in case of a self-equilibrated load at $\eta = 0.75$

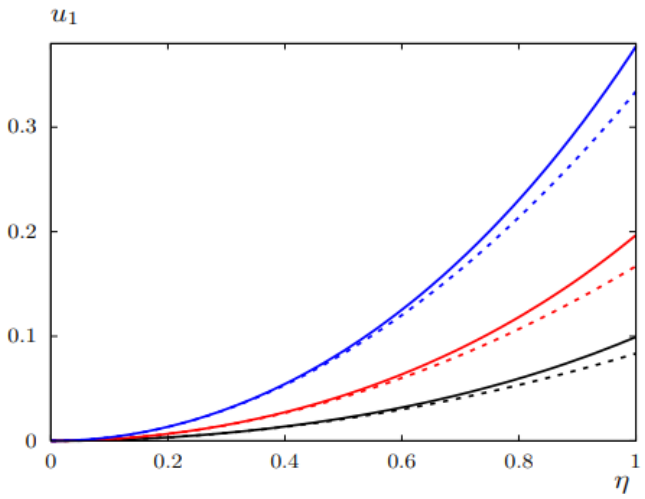

Fig. 7. Comparison of exact (solid lines) and approximate (dotted lines) displacements u_1 versus η for $y_1 = 0.25$ (black), $y_1 = 0.5$ (red), and $y_1 = 1$(blue) in case of a self-equilibrated load

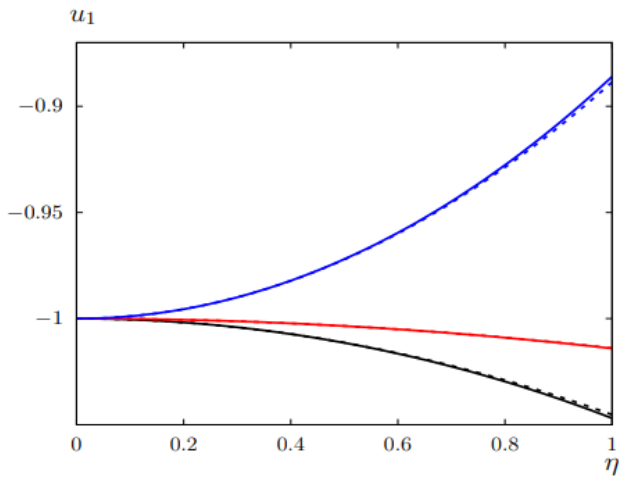

Fig. 8. Comparison of exact (solid lines) and approximate (dotted lines) displacements u_1 vs η for $y_1 = 0.25$ (black), $y_1 = 0.5$ (red), and $y_1 = 1$(blue) in case of a non-self-equilibrated load

The effect of a non-self-equilibrated uniform loading on the horizontal displacement along the y_1-axis is displayed both for approximate and exact formulations in Fig. 6. An apparent parabolic form emerges with the largest displacement arising along the center of the rectangle.

Figures 7 and 8 exhibit the same characteristics as their counterparts for parabolic loading. For a fixed value of the frequency, the displacements grow larger as we move to the edges of the rectangle. The displacements are positive for a self-equilibrated load, see Fig. 7, and they are negative for a non-self-equilibrated load, see Fig. 8. We also note that, as in the case of parabolic loading, the accuracy of approximate formulation is significant, which are displayed against the exact formulation in Figs. 6–8.

5. CONCLUSIONS

A perturbation scheme is implemented to calculate the first order low-frequency corrections to rigid body motions of an elastic rectangle subject to longitudinal forces applied to its opposite faces together with sliding boundary conditions on its upper and lower faces. The leading order solution of the nonhomogeneous harmonic equation corresponds to Newton's second law whereas the next order terms results in a nonhomogeneous biharmonic equation. A similar problem was considered in (Kaplunov and Şahin, 2020); however, the boundary conditions allowed explicit solutions only in the antiplane case and further assumptions had to be imposed in the case of in-plane motions. The sliding boundary considered in this paper, fortunately, allows the variables to be separated resulting in the derivation of an explicit approximate solution for the in-plane displacements of the rectangle. The solution of the next order problem, namely, the nonhomogeneous biharmonic equation, leads to a correction to the classical rigid body dynamics, see eqns. (35) and (36). The obtained corrections to rigid body motions in the low-frequency regime under the action of both self- and non-self-equilibrated loads allow the calculation of the variation of stress and displacement components over the interior of the rectangle. Several figures are presented displaying the variation of displacement components for the derived approximate model along with their exact counterparts. An excellent coincidence between the asymptotic and exact results is observed for a rather large interval of the small parameter η in all figures. It should also be noted that the case of self-equilibrated loading cannot be treated within the classical rigid body model.

The perturbation approach may also be extended to investigate the dynamic response of strongly inhomogeneous layered rectangular structures, see (Prikazchikova et al., 2020), with inner and/or outer sliding boundaries, including anisotropy; multi-span rectangles with contrasting material properties may also be investigated. It is also possible to consider a set of arbitrary stresses applied to opposing sides of the rectangle. The nonlinear structures might also be another promising research area for which the developed model may be employed. In addition, various problems of multi-body dynamics, including calculation of longitudinal forces in railcar dynamics might be taken into account.

APPENDIX. EXACT SOLUTION

In this section, we present the exact solutions of the longitudinal and transverse displacements of the elastic rectangle subject

to time-harmonic parabolic and uniform type end loadings. First, we derive the formulations for the parabolic type end loading.

The equations of motion and boundary conditions given in (1) and (2) can be written in terms of the displacement components, respectively, as:

$$\begin{aligned}&\frac{E(1-\nu)}{(1+\nu)(1-2\nu)}\frac{\partial^2 u_1}{\partial x_1^2}+\frac{E}{2(1+\nu)}\frac{\partial^2 u_1}{\partial x_2^2}+\\&+\frac{E(1-\nu)}{2(1+\nu)(1-2\nu)}\frac{\partial^2 u_2}{\partial x_1\partial x_2}=\rho\frac{\partial^2 u_1}{\partial t^2},\\&\frac{E}{2(1+\nu)}\frac{\partial^2 u_2}{\partial x_1^2}+\frac{E(1-\nu)}{(1+\nu)(1-2\nu)}\frac{\partial^2 u_2}{\partial x_2^2}+\\&+\frac{E(1-\nu)}{2(1+\nu)(1-2\nu)}\frac{\partial^2 u_1}{\partial x_1\partial x_2}=\rho\frac{\partial^2 u_2}{\partial t^2},\end{aligned}\tag{56}$$

and:

$$\begin{aligned}&\frac{E(1-\nu)}{(1+\nu)(1-2\nu)}\frac{\partial u_1}{\partial x_1}\\&\qquad+\frac{E\nu}{(1+\nu)(1-2\nu)}\frac{\partial u_2}{\partial x_2}\Big|_{x_1=\pm l_1}=\\&=M^{\pm}\left(1-\frac{x_2^2}{l_2^2}\right)e^{-i\omega t},\\&\frac{\partial u_1}{\partial x_2}+\frac{\partial u_2}{\partial x_1}\Big|_{x_1=\pm l_1}=0,\\&\frac{\partial u_1}{\partial x_2}+\frac{\partial u_2}{\partial x_1}\Big|_{x_2=\pm l_2}=0,\\&u_2|_{x_2=\pm l_2}.\end{aligned}\tag{57}$$

Considering time-harmonic vibrations together with scaled quantities introduced in (5), the boundary-value problem (56) and (57) may be rewritten as:

$$\begin{aligned}&\kappa^2\frac{\partial^2 u_1^*}{\partial y_1^2}+\delta^2\frac{\partial^2 u_1^*}{\partial y_2^2}+\delta(\kappa^2-1)\frac{\partial^2 u_2^*}{\partial y_1\partial y_2}+\eta^2 u_1^*,\\&\frac{\partial^2 u_2^*}{\partial y_1^2}+\delta^2\kappa^2\frac{\partial^2 u_2^*}{\partial y_2^2}+\delta(\kappa^2-1)\frac{\partial^2 u_1^*}{\partial y_1\partial y_2}+\eta^2 u_2^*,\end{aligned}\tag{58}$$

with:

$$\begin{aligned}&\kappa^2\frac{\partial u_1^*}{\partial y_1}+\delta(\kappa^2-2)\frac{\partial u_2^*}{\partial y_2}\Big|_{y_1=\pm 1}=\eta^2 M_*^{\pm}(1-y_2^2),\\&\delta\frac{\partial u_1^*}{\partial y_2}+\frac{\partial u_2^*}{\partial y_1}\Big|_{y_1=\pm 1}=0,\\&\delta\frac{\partial u_1^*}{\partial y_2}+\frac{\partial u_2^*}{\partial y_1}\Big|_{y_2=\pm 1}=0,\\&u_2^*|_{y_2=\pm 1}\end{aligned}\tag{59}$$

where $\eta=\omega l_1/c_2$.

Let us assume the solutions of (58) are in the form:

$$u_1^*=u_{10}^*+\sum_{n=1}^{\infty}u_{1n}^*(y_1)\cos n\pi y_2,\tag{60}$$

$$u_2^*=\sum_{n=1}^{\infty}u_{2n}^*(y_1)\cos n\pi y_2,$$

see (Kaplunov et al., 2005). Substituting equations (60) into the governing equations and boundary conditions given by (58) and (59) and employing a straightforward but a lengthy algebra we arrive at, omitting all the details:

$$\begin{aligned}u_{10}^*&=-\frac{M_*^+-M_*^-}{3\kappa\sin\frac{\eta}{\kappa}}\eta\cos\left(\frac{\eta}{\kappa}y_1\right)\\&\quad+\frac{M_*^++M_*^-}{3\kappa\cos\frac{\eta}{\kappa}}\eta\sin\left(\frac{\eta}{\kappa}y_1\right),\\u_{1n}^*&=E_1\cosh r_1y_1+E_2\sinh r_1y_1+E_3\cosh r_2y_1\\&\quad+E_4\sinh r_2y_1,\\u_{2n}^*&=-\frac{n\pi\delta E_1}{r_1}\sinh r_1y_1-\frac{n\pi\delta E_2}{r_1}\cosh r_1y_1-\\&\quad-\frac{r_2E_3}{n\pi\delta}\sinh r_2y_1-\frac{r_2E_4}{n\pi\delta}\cosh r_2y_1,\end{aligned}\tag{61}$$

where: $r_1=\pm\sqrt{\delta^2n^2\pi^2-\eta^2/\kappa^2}$, $r_2=\pm\sqrt{\delta^2n^2\pi^2-\eta^2}$, and E_i are the Fourier coefficients given by:

$$\begin{aligned}E_1&=\frac{2\eta^2(n^2\pi^2\delta^2+r_2^2)r_1\cosh r_2\cos n\pi(M_*^+-M_*^-)}{4n^4\pi^4\delta^2r_1r_2\cosh r_1\sinh r_2-n^2\pi^2(n^2\pi^2\delta^2+r_2^2)^2\sinh r_1\cosh r_2},\\E_2&=\frac{2\eta^2(n^2\pi^2\delta^2+r_2^2)r_1\sinh r_2\cos n\pi(M_*^++M_*^-)}{4n^4\pi^4\delta^2r_1r_2\sinh r_1\cosh r_2-n^2\pi^2(n^2\pi^2\delta^2+r_2^2)^2\cosh r_1\sinh r_2},\\E_3&=\frac{-4\eta^2\delta^2r_1\cosh r_1\cos n\pi(M_*^+-M_*^-)}{4n^2\pi^2\delta^2r_1r_2\cosh r_1\sinh r_2-(n^2\pi^2\delta^2+r_2^2)^2\sinh r_1\cosh r_2},\\E_4&=\frac{-4\eta^2\delta^2r_1\sinh r_1\cos n\pi(M_*^++M_*^-)}{4n^2\pi^2\delta^2r_1r_2\sinh r_1\cosh r_2-(n^2\pi^2\delta^2+r_2^2)^2\cosh r_1\sinh r_2}.\end{aligned}\tag{62}$$

The exact solution to the elastic rectangle subject to time-harmonic uniform loading may also be treated similarly. Therefore, leaving out all the algebraic details, the exact formulation for the displacement components are given as:

$$\begin{aligned}u_1^*&=-\frac{\eta(A_*^+-A_*^-)}{2\kappa\sin\frac{\eta}{\kappa}}\cos\frac{\eta}{\kappa}y_1\\&\quad+\frac{\eta(A_*^++A_*^-)}{2\kappa\cos\frac{\eta}{\kappa}}\sin\frac{\eta}{\kappa}y_1,\\u_2^*&=0.\end{aligned}\tag{63}$$

REFERENCES

1. **Babenkova E., Kaplunov J**. (2004), Low-frequency decay conditions for a semi-infinite elastic strip. *Proc. R. Soc. A*., 460(2048), 2153-2169.
2. **Babenkova Y.V., Kaplunov Y.D., Ustinov Y.A**. (2005), Saint-venant's principle in the case of the low-frequency oscillations of a half-strip, *Appl. Math. Mech.*, 69(3), 405-416.
3. **Gregory R.D., Wan F.Y.M**. (1985), On plate theories and Saint-Venant's principle, *International journal of solids and structures*, 21(10), 1005-1024.
4. **Kaplunov J., Prikazchikov D.A., Prikazchikova L.A.**, **Sergushova O.** (2019), The lowest vibration spectra of multi-component structures with contrast material properties, *J. Sound Vib.,* 445, 132-147.

5. **Kaplunov J., Prikazchikov D.A., Rogerson G.A.** (2005), On three-dimensional edge waves in semi-infinite isotropic plates subject to mixed face boundary conditions, *The Journal of the Acoustical Society of America*, 118 (5), 2975-2983.
6. **Kaplunov J., Prikazchikova L., Alkinidri M.** (2021), Antiplane shear of an asymmetric sandwich plate, *Continuum Mechanics and Thermodynamics*, 1-16.
7. **Kaplunov J., Şahin O.** (2020), Perturbed rigid body motions of an elastic rectangle, *Z Angew Math Phys.*, 71(5), 1-15.
8. **Kaplunov J., Shestakova A., Aleynikov I., Hopkins B., Talonov A.** (2015), Low-frequency perturbations of rigid body motions of a viscoelastic inhomogeneous bar, *Mechanics of Time-Dependent Materials*, 19(2), 135-151.
9. **Kudaibergenov A., Nobili A., Prikazchikova L.A.** (2016), On low-frequency vibrations of a composite string with contrast properties for energy scavenging fabric devices, *Journal of Mechanics of Materials and Structures,* 11 (3), 231-243.
10. **Martin T.P., Layman C.N., Moore K.M., Orris G.J.** (2012), Elastic shells with high-contrast material properties as acoustic metamaterial components, *Physical Review B,* 85 (16), 161103.
11. **Milton G.W. and Willis J.R.** (2007), On modifications of Newton's second law and linear continuum elastodynamics, *Proc. R. Soc. A.*, 463 (2079), 855-880.
12. **Prikazchikova L., Aydın Y.E., Erbaş B., Kaplunov J.** (2020), Asymptotic analysis of an anti-plane dynamic problem for a three-layered strongly inhomogeneous laminate, *Math. Mech. Solids,* 25 (1), 3-16.
13. **Qin Y., Wang X., Wang Z.L.** (2008), Microfibre--nanowire hybrid structure for energy scavenging, *Nature,* 451 (7180), 809—813.
14. **Şahin O.** (2019), The effect of boundary conditions on the lowest vibration modes of strongly inhomogeneous beams, *J. Mech. Mater. Struct.*, 14(4), 569-585.
15. **Şahin O., Erbaş B., Kaplunov J., Savsek T.** (2020), The lowest vibration modes of an elastic beam composed of alternating stiff and soft components, *Arch. Appl. Mech.,* 90 (2), 339-352.
16. **Srivastava A., Nemat-Nasser S.** (2012), Overall dynamic properties of three-dimensional periodic elastic composites, *Proc. R. Soc. A.,* 468 (2137), 269-287.
17. **Vigak V.M., Tokovyi Y.V.** (2002), Construction of elementary solutions to a plane elastic problem for a rectangular domain. *International applied mechanics*, 38(7), 829-836.
18. **Viverge K., Boutin C., Sallet F.** (2016), Model of highly contrasted plates ver- sus experiments on laminated glass, *International Journal of Solids and Structures,* 102, 238-258.
19. **Wang X.** (2014), Dynamic behaviour of a metamaterial system with negative mass and modulus, *Int. J. Solids Struct.*, 51(7-8), 1534-1541.
20. **Willis J.R.** (1981), Variational and related methods for the overall properties of composites, In *Advances in applied mechanics*, (21), pp. 1-78, Elsevier.
21. **Willis J.R.** (1981), Variational principles for dynamic problems for inhomogeneous elastic media, *Wave Motion*, 3(1) 1-11.

The authors would like to extend their sincere thanks to J. Kaplunov for the fruitful discussions and his invaluable comments.